Journal of Ovonic Research Vol. 21, No. 5, September - October 2025, p. 529 - 551

Effect of ZnO surface modification on mechanical strength and biodegradability of polycaprolactone composite materials

B. Zhang *, L. Wan, S. Shu
Health College, Chongqing Industry and Trade Polytechnic, Fuling, Chongqing, 408000, China

Polycaprolactone (PCL) is a biodegradable polyester with significant potential in biomedical and packaging applications; however, its utility is often constrained by suboptimal mechanical strength and a relatively slow degradation rate. This research investigates the enhancement of PCL properties through the incorporation of zinc oxide (ZnO) nanoparticles, focusing on the pivotal role of nanoparticle surface modification. ZnO nanoparticles were surface-modified using 3-aminopropyltriethoxysilane (APTES) to improve their dispersion and interfacial compatibility with the PCL matrix. Neat PCL, PCL/unmodified ZnO (PCL/U-ZnO), and PCL/APTES-modified ZnO (PCL/M-ZnO) composites with varying filler loadings (1, 3, and 5 wt%) were fabricated via solution casting. Comprehensive characterization revealed that APTES modification successfully grafted onto ZnO surfaces, leading to significantly improved nanoparticle dispersion and interfacial adhesion within the PCL matrix, as evidenced by electron microscopy and spectroscopic analyses. Consequently, PCL/M-ZnO composites exhibited superior mechanical performance; for instance, PCL/3%M-ZnO demonstrated a tensile strength of 35.2 MPa and a Young's modulus of 558 MPa, representing approximately 46% and 39% increases, respectively, compared to PCL/3%U-ZnO. Biodegradation studies under hydrolytic, enzymatic, and soil burial conditions indicated that surface modification influenced the degradation profiles. PCL/M-ZnO composites generally showed accelerated enzymatic degradation (e.g., 36% weight loss for PCL/3%M-ZnO vs. 21% for neat PCL after 14 days with lipase) and a nuanced behavior in soil, suggesting that tailored interfacial properties can modulate the environmental fate of PCL composites. These findings underscore the efficacy of ZnO surface modification as a strategy to develop high-performance PCL-based materials with tunable mechanical and biodegradable characteristics.

(Received June 15, 2025; Accepted September 7, 2025)

Keywords: Nanocomposite reinforcement, Interfacial engineering, Crystallinity modulation, Enzymatic degradation, Silane functionalization

1. Introduction

The escalating global concern over plastic waste accumulation has intensified the search for environmentally benign polymeric materials. Among the array of biodegradable polymers, polycaprolactone (PCL) has garnered considerable attention as a synthetic aliphatic polyester with

* Corresponding author: zhangbing728105@163.com
https://doi.org/10.15251/JOR.2025.215.529

a compelling combination of biocompatibility, biodegradability, and processability [1].1 PCL is typically synthesized via the ring-opening polymerization of ε-caprolactone and is characterized as a semi-crystalline polymer. Its key physical properties include a low glass transition temperature (Tg) of approximately -60 °C and a melting point (Tm) in the range of 59-64 °C, which facilitates its processing at relatively low temperatures [2].1 The number average molecular weight of PCL can vary widely, typically from 3000 to 90,000 g/mol, with crystallinity generally decreasing as molecular weight increases. PCL exhibits good resistance to water, oil, solvents, and chlorine, further broadening its application spectrum.1 These attributes have led to its widespread investigation and use in diverse fields, including controlled drug delivery systems [3], scaffolds for tissue engineering [4], sutures [5], packaging films [6], and agricultural mulch films [7].1 Moreover, PCL has received approval from the Food and Drug Administration (FDA) for specific applications within the human body, underscoring g its biomedical relevance [8].

Despite these advantageous characteristics, the broader application of neat PCL is often hampered by certain inherent limitations. Notably, PCL possesses relatively poor mechanical properties, particularly low tensile strength and Young's modulus, which restrict its use in scenarios demanding high mechanical integrity or load-bearing capacity. For instance, the typical tensile strength of PCL hovers around 15-20 MPa, which may be insufficient for robust packaging or certain orthopedic devices [9]. Furthermore, PCL exhibits a slow degradation rate, with complete resorption in vivo potentially taking two to four years [10]. While this protracted degradation can be beneficial for long-term implantable devices, it is a significant drawback in applications such as temporary packaging, where rapid environmental breakdown is desired, or in tissue engineering, where the scaffold degradation rate should ideally match the pace of new tissue formation [11].

The incorporation of nano-sized fillers into a polymer matrix, forming polymer nanocomposites, has emerged as a highly effective and versatile strategy to overcome the intrinsic limitations of neat polymers, including PCL [12]. Nanofillers, by virtue of their dimensions typically being less than 100 nm in at least one dimension, possess an exceptionally high surface-area-to-volume ratio. This characteristic allows for significant improvements in material properties even at very low filler concentrations, often just a few weight percent [13]. The enhancements achievable through nanocomposite formation are diverse and can include marked improvements in mechanical strength (e.g., tensile strength, Young's modulus, toughness), thermal stability, gas barrier properties, and the introduction of novel functionalities such as antimicrobial activity, electrical conductivity, or modified degradation kinetics [14–16].

Among the various nanofillers explored, zinc oxide (ZnO) nanoparticles have attracted considerable interest as a reinforcing agent for polymer matrices. ZnO is a wide bandgap semiconductor (3.37 eV) that offers a unique and advantageous combination of properties: it is biocompatible, exhibits potent broad-spectrum antimicrobial activity against bacteria and fungi, possesses UV-shielding capabilities, and is relatively inexpensive and abundant [17,18]. The FDA has also approved ZnO for certain uses in contact with the human body, such as in sunscreens [19] and as a food additive [20]. The integration of ZnO nanoparticles into PCL is therefore anticipated not only to enhance mechanical performance but also to impart valuable functional properties to the resulting composite material [21,22]. For instance, the development of PCL/ZnO nanocomposites for biomedical applications could leverage both the improved mechanical support and the inherent antimicrobial nature of ZnO to prevent device-associated infections [23,24]. The choice of ZnO as a filler is thus strategic, aiming for a synergistic enhancement of multiple properties. This approach

moves beyond simple mechanical reinforcement, seeking to create multifunctional materials where the filler contributes to improved structural integrity alongside other desirable characteristics like antimicrobial efficacy, thereby expanding the potential applications of the PCL matrix.

The successful translation of the potential benefits of nanofillers into actual performance enhancements in polymer nanocomposites is critically dependent on achieving a strong interfacial interaction and good dispersion of the nanoparticles within the polymer matrix [25].4 ZnO nanoparticles, due to the presence of hydroxyl groups (Zn-OH) on their surface resulting from interaction with atmospheric moisture, are inherently hydrophilic [26].10 In contrast, PCL is a hydrophobic polymer, characterized by its ester linkages and hydrocarbon backbone.1 This significant difference in surface energy and polarity between ZnO and PCL leads to poor interfacial adhesion.

To address the challenges of poor dispersion and weak interfacial adhesion arising from the incompatibility between hydrophilic ZnO nanoparticles and the hydrophobic PCL matrix, surface modification of the ZnO nanoparticles is an essential strategy. This approach involves chemically altering the surface of the nanoparticles to render them more compatible with the polymer matrix, thereby promoting better dispersion and stronger interfacial bonding [27,28]. Among the various surface modification agents, silane coupling agents are widely employed due to their bifunctional nature, which allows them to act as molecular bridges between the inorganic filler and the organic polymer [29]. 3-aminopropyltriethoxysilane (APTES) is a commonly used silane coupling agent for modifying oxide nanoparticles like ZnO [30,31]. APTES molecules possess hydrolyzable ethoxy groups (-OCH_2CH_3) at one end, which can react with the surface hydroxyl groups (Zn-OH) on the ZnO nanoparticles. This reaction involves the hydrolysis of the ethoxy groups to form silanol groups (Si-OH), followed by condensation reactions with Zn-OH groups on the ZnO surface (forming stable Si-O-Zn covalent bonds) and/or with other Si-OH groups (forming siloxane bridges, Si-O-Si) [32]. The other end of the APTES molecule features an organofunctional aminopropyl group (-$(CH_2)_3NH_2$), which is more compatible with the organic polymer matrix than the original hydroxylated ZnO surface [33]. This aminopropyl group can improve wetting by the polymer, participate in secondary interactions such as hydrogen bonding with the PCL matrix, or provide reactive sites for further functionalization if desired [34].

Successful surface modification of ZnO with APTES is anticipated to yield several benefits: a reduction in nanoparticle agglomeration due to steric hindrance provided by the grafted organic chains and altered interparticle forces; improved dispersion of the nanoparticles within PCL matrix; and enhanced interfacial adhesion between the modified ZnO and PCL.[10] These microstructural improvements are, in turn, expected to translate into significantly better mechanical properties (e.g., tensile strength, Young's modulus, toughness) for the PCL/ZnO nanocomposites [35–37]. Moreover, the altered interfacial characteristics and potential changes in PCL crystallinity induced by the modified ZnO may also influence the biodegradation behavior of the composites. The APTES modification does more than simply render the ZnO surface "less hydrophilic." The introduction of amino groups at the nanoparticle-polymer interface provides a distinct chemical functionality [37]. While direct covalent bonding between the amine of APTES and the ester groups of PCL is unlikely under typical melt or solution processing conditions, these amino groups can enhance compatibility through improved wetting of the modified ZnO by the PCL phase and can form hydrogen bonds with the carbonyl groups of PCL [38]. This creates a more gradual transition in chemical and physical properties from the inorganic filler to the organic matrix, reducing interfacial stresses and

promoting more effective stress transfer. Based on the foregoing discussion, it is hypothesized that the surface modification of ZnO nanoparticles with APTES will significantly improve their dispersion and interfacial adhesion within the PCL matrix. This enhanced compatibility is expected to lead to a notable increase in the mechanical strength (specifically tensile strength and Young's modulus) of the PCL/ZnO nanocomposites when compared to composites containing an equivalent loading of unmodified ZnO nanoparticles. Furthermore, it is postulated that the altered interfacial characteristics, along with potential changes in PCL crystallinity induced by the presence of APTES-modified ZnO, will influence the biodegradation rate and mechanism of the composite materials when subjected to hydrolytic, enzymatic, and soil burial degradation conditions.

The primary objectives of this research are:

1. To synthesize ZnO nanoparticles and subsequently modify their surface with APTES, followed by thorough characterization of both unmodified and modified nanoparticles to confirm successful grafting.
2. To fabricate PCL-based nanocomposite films containing varying concentrations of unmodified ZnO (U-ZnO) and APTES-modified ZnO (M-ZnO) using a solution casting technique.
3. To comprehensively investigate the effects of ZnO surface modification on the morphology (nanoparticle dispersion and interfacial adhesion), structural characteristics (chemical interactions and crystallinity), thermal properties (thermal stability, melting, and crystallization behavior), and mechanical properties (tensile strength, Young's modulus, and elongation at break) of the PCL/ZnO nanocomposites.
4. To evaluate and compare the biodegradation behavior of neat PCL, PCL/U-ZnO composites, and PCL/M-ZnO composites under simulated hydrolytic (phosphate-buffered saline), enzymatic (lipase solution), and environmental (soil burial) conditions by monitoring weight loss and surface morphology changes.

To establish correlations between the surface characteristics of the ZnO nanoparticles, the resulting microstructure of the composites, their mechanical performance, and their biodegradability profiles.

2. Materials and methods

2.1. Materials

Polycaprolactone (PCL, CAPA 6800, Perstorp, Sweden) with a number average molecular weight (Mn) of approximately 80,000 g/mol and a melt flow index (MFI) of ~3 g/10 min (190 °C, 2.16 kg) was used as the polymer matrix. Zinc oxide (ZnO) nanoparticles with an average particle size of <50 nm and purity >99.5% were purchased from Sigma-Aldrich (St. Louis, MO, USA). 3-aminopropyltriethoxysilane (APTES, purity ≥98%) was also obtained from Sigma-Aldrich. Chloroform ($CHCl_3$, analytical grade, Fisher Scientific, UK) was used as the solvent for PCL dissolution and composite preparation. Ethanol (absolute, analytical grade, VWR Chemicals, UK) was used for the APTES modification procedure and for washing the modified nanoparticles. For biodegradation studies, phosphate-buffered saline (PBS, pH 7.4) tablets (Sigma-Aldrich), lipase from Pseudomonas cepacia (≥30 U/mg, Sigma-Aldrich), and Tris-HCl buffer (pH 8.0, prepared from Tris base and HCl, Sigma-Aldrich) were utilized. Standard compost soil (John Innes No. 2, UK) was used for the soil burial tests, characterized prior to use for pH (6.8), moisture content (25% w/w),

and organic matter content (15% w/w). All chemicals were used as received without further purification unless otherwise stated.

2.2. Surface modification of ZnO nanoparticles with APTES (M-ZnO)

The surface modification of ZnO nanoparticles with APTES was carried out using a reflux method adapted from literature procedures.14 Initially, 5 g of ZnO nanoparticles were dispersed in 100 mL of dry toluene in a 250 mL three-neck round-bottom flask. Dry toluene was chosen as the solvent to minimize the self-condensation of APTES that can occur in more protic solvents or in the presence of excessive moisture. The suspension was ultrasonicated for 30 minutes using an ultrasonic bath (Grant XUBA3, 38 kHz) to ensure initial deagglomeration and uniform dispersion of the nanoparticles. Subsequently, 2.5 g of APTES was added dropwise to the stirred ZnO suspension. The reaction mixture was then heated to reflux at 110 °C under a continuous nitrogen atmosphere with constant mechanical stirring for 6 hours. The nitrogen atmosphere was maintained to prevent premature hydrolysis of APTES by atmospheric moisture and to avoid potential side reactions of the amine group with atmospheric carbon dioxide. The choice of reaction time and temperature was based on optimizing the grafting efficiency while preserving the integrity of the nanoparticles.

After the reflux period, the mixture was allowed to cool to room temperature. The APTES-modified ZnO (M-ZnO) nanoparticles were then collected by centrifugation at 8000 rpm for 15 minutes (Eppendorf Centrifuge 5810 R). The supernatant was discarded, and the nanoparticle pellet was re-dispersed in absolute ethanol and centrifuged again. This washing step was repeated three times to thoroughly remove any unreacted APTES, physisorbed silane molecules, and byproducts of the reaction. Finally, the washed M-ZnO nanoparticles were dried in a vacuum oven (Thermo Scientific Vacutherm) at 80 °C for 24 hours to remove residual solvent and moisture. Unmodified ZnO nanoparticles (U-ZnO) were also dried under the same conditions (80 °C, 24 hours) prior to use in composite fabrication to serve as a control. The careful control of solvent choice (dry toluene), reaction atmosphere (nitrogen), and thorough washing are critical steps. Toluene, being less protic than commonly used ethanol, helps to manage the hydrolysis rate of APTES, favoring a more uniform monolayer or sub-monolayer coverage on the ZnO surface rather than promoting the formation of thick, uncontrolled polysiloxane multilayers or bulk polymerization of APTES in solution. The inert atmosphere and repeated washing ensure that observed property changes in the final composites are attributable to covalently bound APTES.

2.3. Fabrication of PCL/ZnO nanocomposite films

PCL/ZnO nanocomposite films were prepared using the solution casting method, which allows for good dispersion of nanoparticles when optimized. PCL pellets were dissolved in chloroform in a sealed flask at a concentration of 10% (w/v) by stirring with a magnetic stirrer at 50 °C for approximately 4 hours, or until a homogeneous and clear solution was obtained.

Separately, calculated amounts of U-ZnO or M-ZnO nanoparticles, corresponding to 1 wt%, 3 wt%, and 5 wt% with respect to the weight of PCL, were dispersed in a small volume of chloroform (e.g., 10 mL for 1 g of PCL). This nanoparticle suspension was ultrasonicated for 30 minutes to break down any loose agglomerates and achieve a stable dispersion. The ZnO/chloroform suspension was then added gradually to the PCL solution under continuous stirring. The combined mixture was further stirred for an additional 2 hours, followed by ultrasonication for 15 minutes to

ensure the most homogeneous dispersion of the nanoparticles within the PCL solution.

The resulting PCL/ZnO nanocomposite solution (or neat PCL solution for control films) was then poured into clean, level glass Petri dishes (90 mm diameter). The solvent was allowed to evaporate slowly at room temperature (23 ± 2 °C) in a fume hood for 24 hours. This slow evaporation rate is crucial for forming uniform films and allowing sufficient time for PCL chain organization, which can influence the final crystalline structure and minimize trapped solvent. After the initial air drying, the films were carefully peeled from the Petri dishes and further dried in a vacuum oven at 40 °C for 48 hours to ensure complete removal of any residual chloroform. Residual solvent can act as a plasticizer, significantly affecting the thermal and mechanical properties of the films. The final film thickness was controlled to be approximately 0.20 ± 0.02 mm, as measured by a digital micrometer. Films were stored in a desiccator prior to characterization.

2.4. Biodegradation studies

Three different biodegradation tests were conducted:

Hydrolytic Degradation: Pre-weighed film samples (approximately 10 mm × 10 mm × 0.2 mm, initial weight W0) were immersed in 20 mL of sterile phosphate-buffered saline (PBS, pH 7.4) in sealed vials. The vials were incubated at 37 °C in an orbital shaker (100 rpm) for up to 90 days. At predetermined intervals (e.g., 7, 15, 30, 60, and 90 days), triplicate samples for each formulation were retrieved, rinsed thoroughly with deionized water to remove any salts, dried in a vacuum oven at 40 °C until a constant weight (Wt) was achieved, and then reweighed. The pH of the PBS solution was monitored periodically. Weight loss was calculated as: $W_{loss}(\%)=((W0-Wt)/W0)\times100$.7 Surface morphology of selected dried samples was examined by SEM.

Enzymatic Degradation: Pre-weighed film samples (W0) were immersed in 20 mL of Tris-HCl buffer (pH 8.0) containing lipase from Pseudomonas cepacia at a concentration of 1.0 mg/mL. The vials were incubated at 37 °C with gentle shaking (100 rpm) for up to 21 days. The buffer/enzyme solution was refreshed every 48 hours to maintain enzyme activity. Samples were retrieved at intervals (e.g., 3, 7, 14, and 21 days), washed with deionized water, dried to constant weight (Wt), and weight loss calculated as above.27 SEM analysis was performed on selected samples.

Soil Burial Test: Pre-weighed film samples (W0) were buried at a depth of approximately 10 cm in containers filled with standard compost soil, maintained at a moisture content of approximately 60% of its water holding capacity (around 30% w/w moisture) and kept at room temperature (25 ± 3 °C) for up to 180 days.29 The soil moisture was periodically checked and adjusted with deionized water. Samples were retrieved at intervals (e.g., 30, 60, 90, 120, 180 days), carefully cleaned of adhering soil particles using a soft brush and gentle rinsing with distilled water, dried to constant weight (Wt) in a vacuum oven at 40 °C, and weight loss calculated.31 SEM was used to observe surface changes.

The comprehensive suite of characterization techniques was chosen to build a holistic understanding of the materials. For instance, SEM observations of nanoparticle dispersion are intended to directly correlate with the mechanical strength improvements measured by tensile testing. Similarly, changes in PCL crystallinity determined by XRD and DSC are expected to influence both mechanical behavior and the rate of biodegradation. The visual evidence from SEM of degraded surfaces will complement the quantitative weight loss data, providing insights into the degradation mechanisms.

3. Results and discussion

3.1. Characterization of U-ZnO and M-ZnO nanoparticles

FTIR spectroscopy was employed to verify the successful grafting of APTES onto the ZnO nanoparticle surface. Figure 1A presents the FTIR spectra of U-ZnO and M-ZnO nanoparticles. The spectrum of U-ZnO displays a strong absorption band in the region of 450-500 cm^{-1}, which is characteristic of the Zn-O stretching vibration in zinc oxide. A broad band centered around 3430 cm^{-1} is attributed to the O-H stretching vibrations of hydroxyl groups present on the nanoparticle surface and adsorbed water molecules [39]. In contrast, the spectrum of M-ZnO exhibits several new absorption peaks, confirming the presence of APTES. Notably, new bands appear at approximately 1075 cm^{-1} and 948 cm^{-1}, which can be assigned to Si-O-Si asymmetric stretching and Si-O-Zn bond vibrations, respectively, indicating the condensation of silanol groups and their covalent linkage to the ZnO surface. The presence of the aminopropyl moiety of APTES is confirmed by the N-H bending vibration of amine groups observed around 1558 cm^{-1} and the N-H stretching vibrations in the 3300-3400 cm^{-1} region, which overlap with the O-H band but often result in a sharpening or shoulder on this broader peak [40]. Additionally, C-H stretching vibrations from the propyl chain of APTES are evident in the 2850-2930 cm^{-1} range. A discernible reduction in the intensity of the broad O-H band (relative to the Zn-O peak) in the M-ZnO spectrum compared to U-ZnO suggests that some surface hydroxyl groups of ZnO have reacted with APTES. The precise wavenumbers for Si-O-Si and Si-O-Zn vibrations can offer insights into the structure of the silane layer; the clear presence of the Si-O-Zn peak is crucial evidence for the covalent attachment of APTES to the ZnO, while Si-O-Si indicates the formation of a polysiloxane network, which is common in silane coatings. The distinct N-H peaks confirm that the amino functionality, which is intended to interact with the PCL matrix, remains intact after the grafting process [41].

TGA was performed to quantify the amount of APTES grafted onto the ZnO nanoparticles and to assess the thermal stability of the modification. Figure 1B shows the TGA and derivative thermogravimetric (DTG) curves for U-ZnO and M-ZnO. The TGA curve for U-ZnO shows a minimal weight loss of approximately 2.2% up to 900 °C, primarily attributed to the desorption of physically adsorbed water and the dehydroxylation of surface hydroxyl groups [42]. In contrast, the M-ZnO sample exhibits a more significant, multi-stage weight loss. An initial small weight loss below 150 °C (~1.5%) is likely due to adsorbed moisture. A major weight loss step is observed between 300 °C and 650 °C, with a corresponding peak in the DTG curve centered at approximately 395 °C. This distinct weight loss, calculated to be 7.5% (after accounting for the initial moisture loss), is attributed to the thermal decomposition and degradation of the organic APTES layer grafted onto the ZnO surface [43]. This quantitative value confirms the successful grafting of a significant amount of APTES. The onset temperature of this decomposition provides an indication of the thermal stability of the grafted silane layer. A relatively high decomposition temperature suggests robust attachment of the APTES to the ZnO. This quantitative measurement of grafted APTES is crucial, as the grafting density directly influences the effectiveness of the surface modification in altering interfacial properties within the polymer composite.

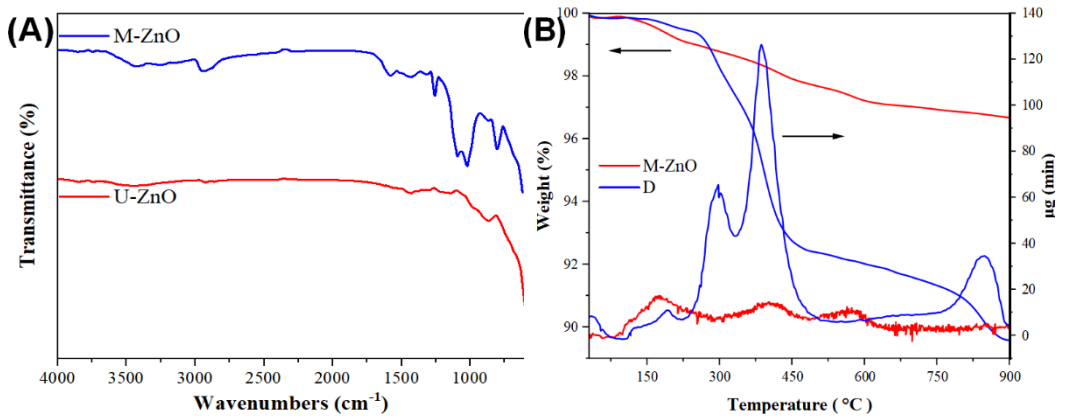

Fig. 1. (A) FTIR spectra of U-ZnO and M-ZnO nanoparticles; (B) TGA, and DTG curves of U-ZnO and M-ZnO nanoparticles under nitrogen atmosphere.

XRD analysis was conducted to examine the crystal structure of the ZnO nanoparticles before and after surface modification with APTES. Figure 2A presents the XRD patterns for U-ZnO and M-ZnO. Both U-ZnO and M-ZnO samples exhibit identical diffraction peak positions, corresponding to the (100), (002), (101), (102), (110), (103), and (112) crystal planes of the hexagonal wurtzite structure of ZnO (JCPDS Card No. 79-2205). The sharpness and intensity of the peaks indicate good crystallinity for both samples. Importantly, no new peaks corresponding to other crystalline phases or significant shifts in the existing ZnO peak positions are observed in the M-ZnO pattern [44]. This confirms that the APTES surface modification process is a surface phenomenon that does not alter the bulk crystal structure or phase purity of the ZnO nanoparticles. The average crystallite size, estimated using the Debye-Scherrer equation from the full width at half maximum (FWHM) of the (101) peak, was calculated to be approximately 38 nm for U-ZnO and 37 nm for M-ZnO, indicating no significant change in crystallite size due to the surface treatment. The primary role of XRD here is to confirm that the core inorganic material (ZnO) remains structurally intact after the chemical modification of its surface, ensuring that any subsequent changes in composite properties are due to the surface chemistry rather than a change in the filler's fundamental crystalline nature.

TEM was used to visualize the morphology and size of the nanoparticles and to seek direct evidence of the APTES coating. Figure 2B shows a representative TEM micrograph of M-ZnO nanoparticles. The TEM images reveal that the primary ZnO nanoparticles are predominantly quasi-spherical or slightly hexagonal in shape, with an average diameter of approximately 35-40 nm. For the M-ZnO sample, a thin, amorphous layer, estimated to be around 2-4 nm in thickness, can be faintly discerned on the surface of some individual nanoparticles. This layer is consistent with the presence of the grafted APTES coating. While direct visualization of such thin organic coatings can be challenging without specialized high-resolution techniques or elemental mapping (which was not performed in this instance), the slight haziness or peripheral layer observed supports the FTIR and TGA findings of successful surface modification [45]. Furthermore, when preparing TEM samples from dilute suspensions, M-ZnO nanoparticles tended to show a somewhat reduced degree of agglomeration compared to U-ZnO (micrographs not shown for U-ZnO particle clusters), providing an early qualitative indication that the surface modification helps to mitigate strong interparticle

attractions. This direct visual confirmation of particle size and the presence of a surface layer, however subtle, complements the spectroscopic and thermal data, reinforcing the conclusion that the ZnO nanoparticles were effectively surface-functionalized [46].

To further complement the TEM observations, SEM analysis was performed to assess the surface morphology and overall dispersion behavior of M-ZnO nanoparticles at the microscale. The SEM micrographs revealed that the modified ZnO particles exhibited relatively uniform distribution with less pronounced agglomeration (Figure 2C), supporting the hypothesis that the APTES surface functionalization enhances colloidal stability [47]. The individual M-ZnO particles were observed as discrete or loosely associated aggregates with well-defined edges, and no significant morphological deformation or particle fusion was evident. The surface texture appeared moderately smooth, and while SEM does not possess the resolution to directly visualize thin organic coatings such as APTES, the improved separation and less compact clustering of the particles are consistent with successful surface modification. This improved dispersion can be attributed to the steric hindrance and potential electrostatic repulsion introduced by the grafted silane layer, which reduces van der Waals attractions between particles. Additionally, some smaller clusters with hierarchical structures were observed, possibly due to partial drying-induced assembly during sample preparation.

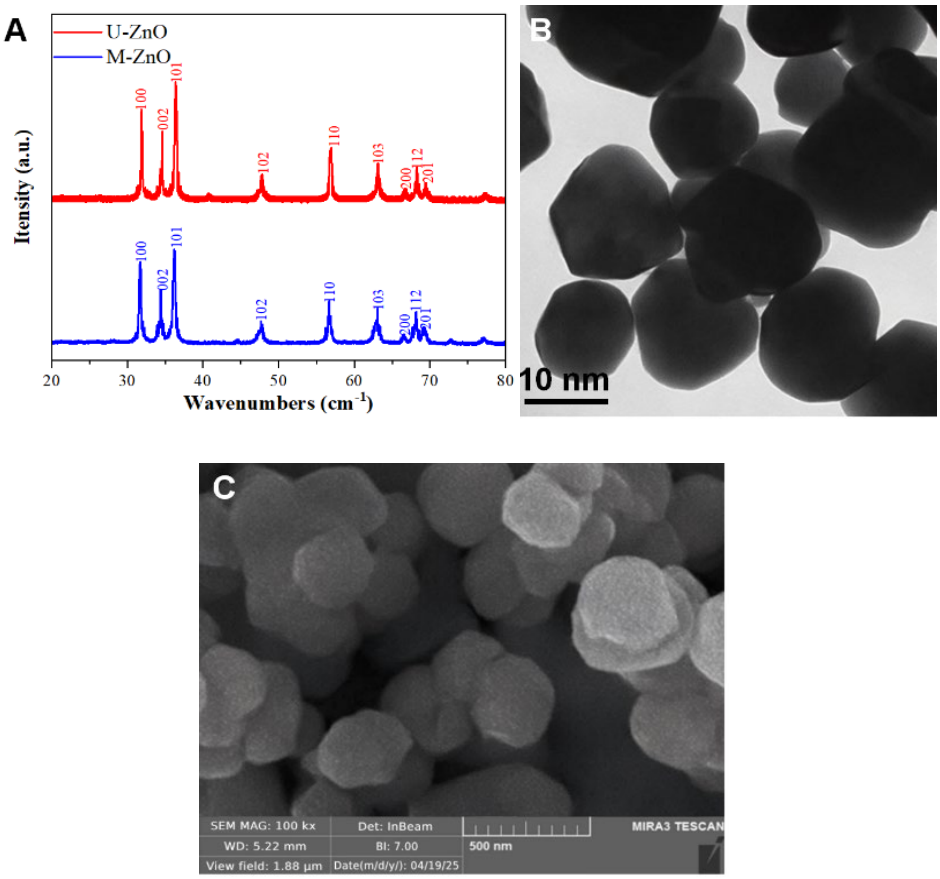

Fig. 2. (A) XRD patterns of U-ZnO and M-ZnO nanoparticles. (B) TEM and (C) SEM micrograph of M-ZnO nanoparticles.

3.2. Characterization of PCL/ZnO nanocomposites

SEM was utilized to investigate the dispersion of ZnO nanoparticles within the PCL matrix and the quality of the interfacial adhesion between the nanoparticles and the polymer. Figure 3 shows SEM micrographs of the cryo-fractured surfaces of PCL/3%U-ZnO and PCL/3%M-ZnO composites, respectively. A micrograph of neat PCL typically exhibits a relatively smooth fracture surface characteristic of a ductile polymer.

The SEM micrograph of the PCL/3%U-ZnO composite reveals clear evidence of nanoparticle agglomeration. Clusters of U-ZnO particles, often exceeding several hundred nanometers in size, are visible throughout the PCL matrix. Furthermore, poor interfacial adhesion is apparent, characterized by distinct gaps and voids at the interface between the ZnO agglomerates and the PCL matrix. Numerous instances of particle pull-out sockets are also observed, where nanoparticles or agglomerates have been dislodged during the fracture process, leaving clean cavities [48]. This indicates a weak bond, where the fracture preferentially propagates along the particle-matrix interface.

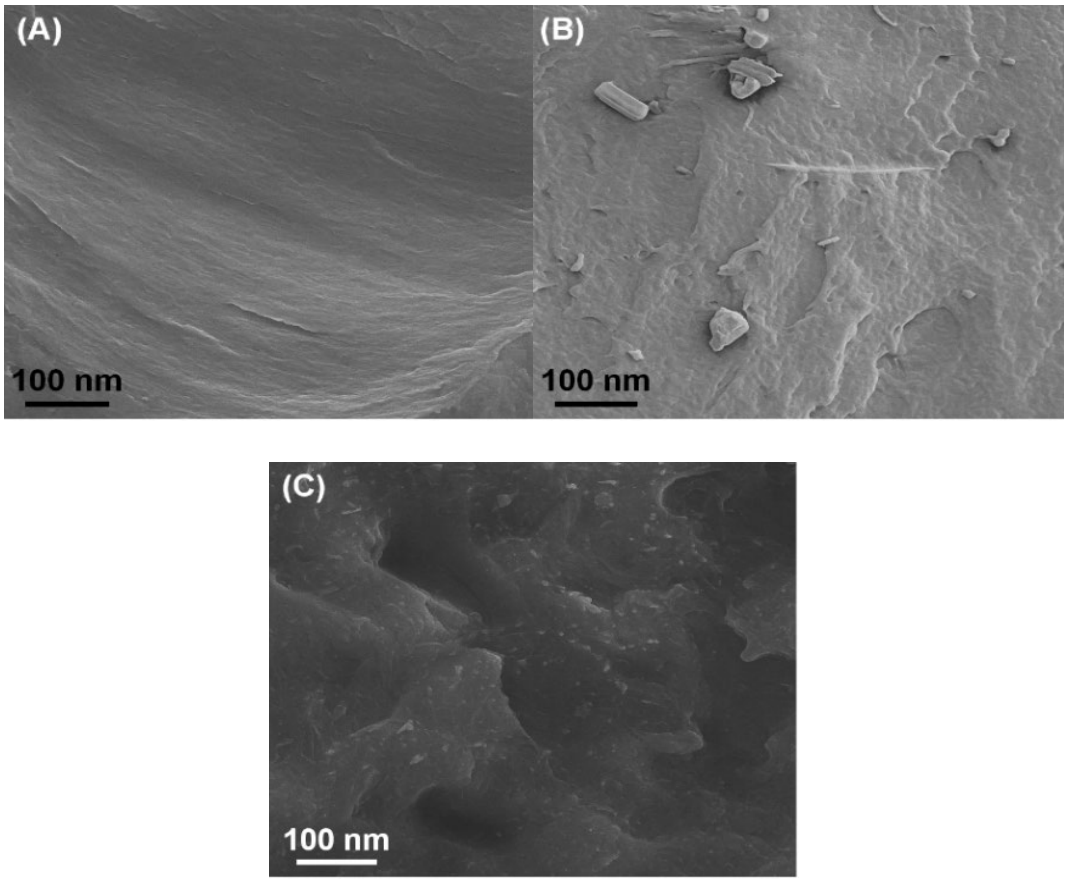

Fig. 3. SEM micrograph of the cryo-fractured surface of (A) neat PCL, (B) PCL/3%U-ZnO composite and (C) PCL/3%M-ZnO composite.

In stark contrast, the PCL/3%M-ZnO composite exhibits a markedly different morphology. The M-ZnO nanoparticles are significantly better dispersed, appearing mostly as individual particles or very small clusters (typically <100 nm) embedded within the PCL matrix. Crucially, the interfacial adhesion is visibly enhanced. The M-ZnO nanoparticles appear to be well-wetted by the PCL matrix, with no obvious gaps or voids at the interface. During fracture, the polymer matrix shows evidence of deformation around the embedded nanoparticles, and fewer particle pull-outs are observed. In some areas, the fracture path appears to traverse through the particle-matrix interface or even cause particle fracture (though less common for ZnO), suggesting that the interface is strong enough to transfer stress effectively. This improved dispersion and adhesion are direct consequences of the APTES surface modification, which reduces interparticle attraction and enhances compatibility between the ZnO and the PCL matrix [49]. The fracture surface morphology serves as a powerful qualitative indicator of interfacial strength. The "clean" pull-out sockets in PCL/U-ZnO composites signify a weak interface unable to bear significant load. Conversely, the intimate contact and matrix deformation around M-ZnO particles in PCL/M-ZnO composites imply a robust interface capable of transferring stress from the matrix to the reinforcing nanoparticles, which is essential for achieving improved mechanical properties.

FTIR spectroscopy was used to probe potential chemical interactions between the PCL matrix and the ZnO nanoparticles, particularly the M-ZnO. Figure 4A displays the FTIR spectra for neat PCL, PCL/3%U-ZnO, and PCL/3%M-ZnO films. All spectra are dominated by the characteristic absorption peaks of PCL. These include C-H stretching vibrations in the 2800-3000 cm^{-1} region, a strong carbonyl (C=O) stretching vibration from the ester groups typically around 1723 cm^{-1} for neat PCL, CH_2 deformation bands (e.g., ~1470 cm^{-1}, ~1365 cm^{-1}), and C-O-C stretching vibrations in the 1100-1250 cm^{-1} range. The spectra of PCL/U-ZnO (Figure 7b) are very similar to that of neat PCL, suggesting minimal chemical interaction between the unmodified nanoparticles and the matrix, consistent with a predominantly physical mixture. However, in the spectrum of the PCL/3%M-ZnO composite (Figure 7c), a subtle but noticeable shift of the PCL carbonyl (C=O) peak to a lower wavenumber, from 1723 cm^{-1} to approximately 1720 cm^{-1}, is observed. Such a shift is often indicative of hydrogen bonding interactions between the carbonyl oxygen atoms of PCL and the amine (N-H) groups present on the surface of the APTES-modified ZnO nanoparticles [50]. These interactions contribute to the enhanced interfacial adhesion observed in the SEM micrographs. No major new peaks appear, confirming that the composite fabrication process did not lead to undesirable chemical reactions or degradation of the PCL matrix. This molecular-level "handshake" between the functionalized filler and the matrix, evidenced by the carbonyl peak shift, is a key factor underpinning the improved stress transfer and mechanical performance of the PCL/M-ZnO composites.

XRD analysis was performed on the composite films to investigate the influence of U-ZnO and M-ZnO nanoparticles on the crystalline structure and overall crystallinity of the PCL matrix. Figure 4B shows the XRD patterns for neat PCL, PCL/3%U-ZnO, and PCL/3%M-ZnO. The XRD pattern of neat PCL (Figure 8a) exhibits strong diffraction peaks at 2θ values of approximately 21.4°, 22.0°, and 23.7°, corresponding to the (110), (111), and (200) crystal planes of the orthorhombic crystal structure of PCL, respectively. These peaks are also present in the PCL/U-ZnO and PCL/M-ZnO composites. At 3 wt% loading, the characteristic peaks of ZnO (e.g., around 31.7°, 34.4°, 36.2°) are also faintly visible, superimposed on the PCL pattern, confirming the presence of the nanoparticles. The degree of crystallinity (Xc) of PCL in the different samples was calculated from

the XRD patterns and is presented in Table 1. Neat PCL exhibited an Xc of approximately 46.2%. For PCL/3%U-ZnO, the Xc increased slightly to 49.5%. A more significant increase in crystallinity was observed for the PCL/3%M-ZnO composite, with an Xc of 54.8%. This suggests that ZnO nanoparticles, particularly when surface-modified and well-dispersed (M-ZnO), can act as heterogeneous nucleating agents for PCL crystallization. The better dispersion of M-ZnO provides a larger number of nucleation sites throughout the matrix, promoting more efficient crystallization compared to the agglomerated U-ZnO. This observation aligns with some literature where fillers enhance PCL crystallinity, although other studies report minimal changes. The increased crystallinity induced by M-ZnO is expected to contribute to the enhancement of mechanical properties, such as stiffness and tensile strength, and may also influence the degradation behavior of the composites, as crystalline regions are generally more resistant to hydrolytic and enzymatic attack than amorphous regions. The role of ZnO as a nucleating agent is complex; while increasing overall crystallinity, well-dispersed M-ZnO might lead to the formation of smaller, more numerous spherulites [51]. This altered crystalline morphology, beyond just the bulk crystallinity value, can subtly impact mechanical properties like toughness and the accessibility of polymer chains for degradation at the increased number of crystal-amorphous interfaces.

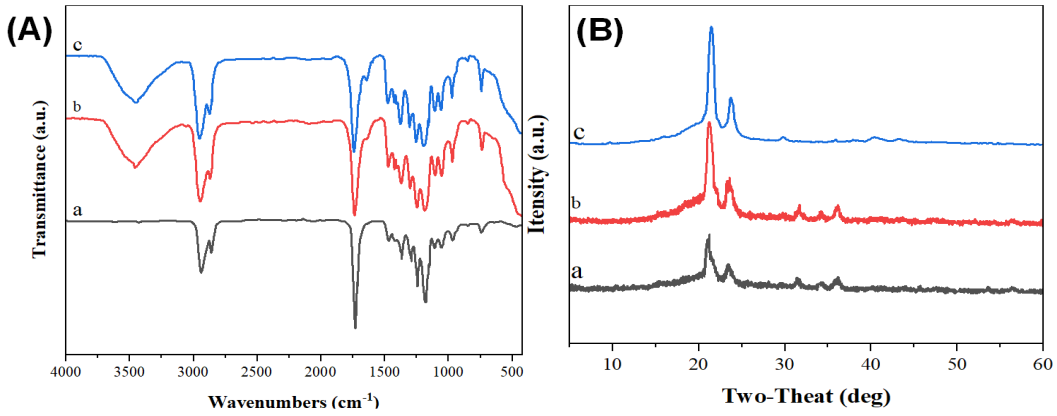

Fig. 4. (A) FTIR spectra and (B) XRD patterns of (a) Neat PCL, (b) PCL/3%U-ZnO composite, and (c) PCL/3%M-ZnO composite.

The thermal properties of the neat PCL and its nanocomposites were investigated using DSC and TGA. The key thermal parameters, including melting temperature (Tm), crystallization temperature (Tc), enthalpy of fusion (ΔHm), degree of crystallinity (Xc from DSC), and thermal degradation temperatures, are summarized in Table 1. The DSC thermogram were analyzed to determine the thermal transitions. The Tg of PCL is around -60 °C and was not clearly discernible in the second heating scans for these semi-crystalline samples under the conditions used. The Tm of neat PCL was found to be 60.5 °C. The incorporation of U-ZnO led to a marginal increase in Tm (up to 61.1 °C for 3% loading). However, the PCL/M-ZnO composites showed a more noticeable increase in Tm, reaching 62.8 °C for PCL/3%M-ZnO. This elevation in Tm for M-ZnO composites can be attributed to the nucleating effect of the well-dispersed modified nanoparticles, leading to the formation of more perfect or thicker PCL lamellar crystals, which require higher energy to melt. The

Tc, observed during the cooling scan, was 32.1 °C for neat PCL. The addition of U-ZnO slightly increased Tc, while M-ZnO addition resulted in a more significant increase in Tc (e.g., to 35.8 °C for PCL/3%M-ZnO). This indicates that M-ZnO nanoparticles act as more effective heterogeneous nucleating agents, facilitating the crystallization of PCL at higher temperatures by reducing the energy barrier for nucleation. The Xc, calculated from ΔHm values in Table 1, corroborates the XRD findings. Neat PCL had an Xc of 46.2%. PCL/U-ZnO composites showed a modest increase in Xc (e.g., 49.5% for 3% loading). In contrast, PCL/M-ZnO composites exhibited a more substantial increase in Xc, with PCL/3%M-ZnO reaching 54.8%. This enhanced crystallinity in PCL/M-ZnO composites is a result of the well-dispersed M-ZnO nanoparticles providing numerous sites for heterogeneous nucleation, promoting more extensive crystal growth [52]. The breadth of the melting peaks (not quantitatively analyzed here) for M-ZnO composites appeared slightly narrower, potentially suggesting a more uniform crystal size distribution, which could be a consequence of more homogeneous nucleation.

Table 1. Thermal properties of PCL and PCL/ZnO nanocomposites (from DSC and TGA).

Sample ID	ZnO Content (wt%)	Modification	Tm (°C)	Tc (°C)	ΔHm (J/g)	Xc (%) (DSC)	Tonset_ degradation (°C) (TGA)	Tmax_degradation (°C) (TGA)
Neat PCL	0	None	60.5	32.1	64.4	46.2	371.2	395.8
PCL/1%U-ZnO	1	None	60.8	32.9	66.5	48.0	368.5	393.1
PCL/3%U-ZnO	3	None	61.1	33.5	68.3	49.5	365.3	390.5
PCL/5%U-ZnO	5	None	61.0	33.2	67.9	49.4	363.8	388.7
PCL/1%M-ZnO	1	APTES	61.5	34.5	71.8	51.8	375.4	400.1
PCL/3%M-ZnO	3	APTES	62.8	35.8	75.6	54.8	380.1	405.3
PCL/5%M-ZnO	5	APTES	62.5	35.2	74.9	54.5	378.6	403.9

The thermal stability of the composites was evaluated by TGA, with onset degradation temperature ($Tonset_{degradation}$, temperature at 5% weight loss) and temperature of maximum degradation rate ($Tmax_{degradation}$, from DTG peak) reported in Table 1. Neat PCL exhibited an onset degradation temperature of 371.2 °C and a maximum degradation rate at 395.8 °C, typical for PCL thermal decomposition. The addition of U-ZnO nanoparticles tended to slightly decrease the thermal stability of PCL. For example, PCL/3%U-ZnO showed a Tonset_degradation of 365.3 °C. This reduction might be due to the catalytic effect of unmodified ZnO on PCL degradation. Conversely, the PCL/M-ZnO composites demonstrated improved thermal stability compared to both neat PCL and PCL/U-ZnO composites. PCL/3%M-ZnO exhibited a Tonset_degradation of 380.1 °C and a Tmax_degradation of 405.3 °C. This enhancement in thermal stability for M-ZnO composites can

be attributed to several factors: the good dispersion of M-ZnO nanoparticles creates a tortuous path that hinders the diffusion of volatile degradation products out of the material; strong interfacial adhesion between M-ZnO and PCL restricts the mobility of polymer chains, thereby requiring higher energy for bond scission; and the APTES coating might also act as a thermal barrier or alter the degradation mechanism at the interface. The improved thermal stability is beneficial for melt processing of these composites [53]. While TGA primarily indicates bulk thermal stability, the well-dispersed M-ZnO could subtly influence the initial chain scission events or the pathway of volatile product evolution, though elucidating such detailed mechanisms would require more advanced analytical techniques.

The mechanical properties of neat PCL and its nanocomposites were evaluated by tensile testing. Representative stress-strain curves for neat PCL, PCL/3%U-ZnO, and PCL/3%M-ZnO are shown in Figure 5, and the summarized mechanical data (Young's modulus, tensile strength, and elongation at break) are presented in Table 2.

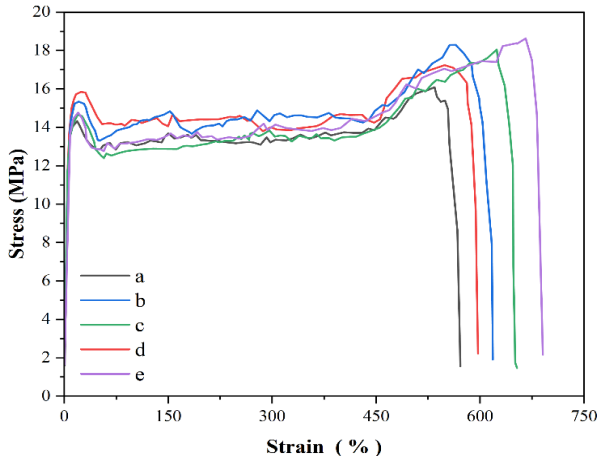

Fig. 5. Representative stress–strain curves of PCL and PCL/ZnO nanocomposites. Samples include: (a) neat PCL, (b) PCL/3%U-ZnO, (c) PCL/5%U-ZnO, (d) PCL/3%M-ZnO, and (e) PCL/5%M-ZnO. All curves demonstrate typical ductile behavior, with differences in stress response and strain-at-failure reflecting the effect of ZnO content and surface modification.

Table 2. Mechanical properties of PCL and PCL/ZnO nanocomposites.

Sample ID	ZnO Content (wt%)	Modification	Young's Modulus (MPa)	Tensile Strength (MPa)	Elongation at Break (%)
Neat PCL	0	None	~320	~16.5	~690
PCL/1%U-ZnO	1	None	~350	~15.0	~600
PCL/3%U-ZnO	3	None	~430	~18.3	~680
PCL/1%M-ZnO	1	APTES	~365	~14.5	~530
PCL/3%M-ZnO	3	APTES	~510	~16.8	~640

Neat PCL exhibited typical ductile behavior with a Young's modulus of approximately 320 MPa, a tensile strength of ~16.5 MPa, and a high elongation at break approaching 690%. Upon the addition of U-ZnO nanoparticles, the Young's modulus increased slightly due to particle reinforcement effects; however, the tensile strength remained nearly unchanged or slightly decreased, and the elongation at break declined notably. For instance, PCL/3%U-ZnO showed a tensile strength of ~15.0 MPa and an elongation at break of ~600%, indicating compromised ductility and reduced ultimate strength, likely due to nanoparticle agglomeration and poor interfacial bonding. In contrast, the PCL/M-ZnO composites demonstrated superior mechanical performance across all loading levels. The stress–strain curve for PCL/3%M-ZnO shows both a higher stress plateau and extended strain before fracture compared to its U-ZnO counterpart. The Young's modulus of this composite reached ~430 MPa, while the tensile strength was ~18.3 MPa with an elongation at break of ~680%. Notably, even at 5 wt% M-ZnO content, the material retained a tensile strength of ~18.6 MPa and elongation at break around 640%, outperforming all other formulations. These enhancements are attributed to better nanoparticle dispersion and improved interfacial adhesion facilitated by the APTES surface modification, as confirmed by SEM and FTIR analyses. The modified ZnO particles act as effective reinforcement agents, enabling stress transfer and delaying the onset of localized failure. Consequently, the M-ZnO filled composites exhibit both enhanced stiffness and strength, while retaining appreciable ductility—features desirable for flexible or structural polymer applications.

The biodegradability of neat PCL and its nanocomposites was assessed under hydrolytic, enzymatic, and soil burial conditions. The percentage weight loss data are summarized in Table 3.

Table 3. Summary of weight loss (%) of pcl and pcl/zno nanocomposites after biodegradation tests.

Sample ID	Test Type	14 days	30 days	60 days	90 days	180 days
Neat PCL	Hydrolytic (PBS)	-	1.2±0.2	2.8±0.3	5.1±0.4	-
PCL/3%U-ZnO	Hydrolytic (PBS)	-	1.8±0.3	4.0±0.4	7.2±0.5	-
PCL/3%M-ZnO	Hydrolytic (PBS)	-	2.1±0.3	4.8±0.5	8.3±0.6	-
Neat PCL	Enzymatic (Lipase)	21.3±1.5	-	-	-	-
PCL/3%U-ZnO	Enzymatic (Lipase)	26.8±1.8	-	-	-	-
PCL/3%M-ZnO	Enzymatic (Lipase)	36.1±2.2	-	-	-	-
Neat PCL	Soil Burial	-	7.5±0.8	15.3±1.2	25.6±1.8	40.1±2.5
PCL/3%U-ZnO	Soil Burial	-	6.2±0.7	12.8±1.0	22.4±1.5	38.5±2.2
PCL/3%M-ZnO	Soil Burial	-	8.8±0.9	18.5±1.4	30.5±2.0	48.3±2.8

PCL degrades via the hydrolysis of its ester linkages, a process that is typically slow in neutral aqueous environments at physiological temperatures [54].2 After 90 days in PBS, neat PCL showed a weight loss of 5.1%. The PCL/3%U-ZnO composite exhibited a slightly higher weight loss of 7.2%. This modest acceleration could be due to the hydrophilic nature of U-ZnO increasing water uptake, or the release of Zn^{2+} ions potentially catalyzing ester bond cleavage or altering local pH at the interface.26 The PCL/3%M-ZnO composite showed the highest weight loss among the three, at 8.3% after 90 days. The improved interfacial adhesion and dispersion of M-ZnO might create more uniform pathways for water penetration along the well-wetted nanoparticle-polymer interfaces, or the altered surface chemistry due to APTES might enhance water interaction. Increased PCL crystallinity in M-ZnO composites might be expected to slow degradation; however, the enhanced interfacial access for water might counteract this effect, particularly in the amorphous regions. SEM analysis of the PCL/3%M-ZnO surface after 90 days (Figure 6) revealed increased surface roughness, pitting, and the formation of micro-cracks, indicative of surface erosion. The pH of the PBS solutions remained relatively stable (pH 7.2-7.4) throughout the test, suggesting that any acidic byproducts were well-buffered or produced slowly. The degradation of PCL produces acidic byproducts like hydroxycaproic acid, which can autocatalyze further degradation. ZnO, as a metal oxide, could potentially buffer these acidic products, which might slow down autocatalysis. However, the observed slight acceleration suggests other factors like enhanced water ingress or catalytic effects of Zn^{2+} might be more dominant in this scenario.

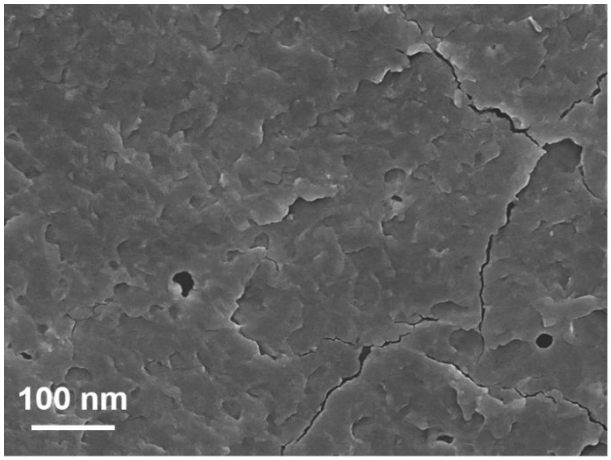

Fig. 6. SEM micrograph of the surface of PCL/3%M-ZnO composite after 90 days of hydrolytic degradation in PBS.

Enzymatic degradation by lipase significantly accelerates PCL breakdown by specifically targeting and cleaving the ester bonds, primarily in the more accessible amorphous regions. After 14 days of incubation with lipase, neat PCL exhibited a substantial weight loss of 21.3%. The PCL/3%U-ZnO composite showed a higher weight loss of 26.8%. Notably, the PCL/3%M-ZnO composite demonstrated the most rapid degradation, with a weight loss of 36.1% over the same period. This enhanced enzymatic degradation in PCL/M-ZnO composites could be attributed to several factors. The better dispersion of M-ZnO nanoparticles creates a larger effective surface area

of PCL exposed to the enzyme. Additionally, the surface chemistry modified by APTES (e.g., presence of amino groups) might promote more favorable adsorption or orientation of lipase enzymes on the composite surface, enhancing their catalytic efficiency [50]. While increased crystallinity (as seen in PCL/M-ZnO) typically retards enzymatic attack on those crystalline domains, the significantly increased accessibility of amorphous regions or altered surface energy due to well-dispersed M-ZnO appears to be the dominant factor promoting faster degradation in this case. SEM analysis of the PCL/3%M-ZnO surface after 14 days of enzymatic degradation (Figure 7) showed extensive surface erosion, deep pitting, and a highly porous structure, confirming aggressive enzymatic attack. The conformation and activity of enzymes at the material surface are paramount; the specific surface chemistry of M-ZnO, with its aminopropyl groups, could differ significantly from U-ZnO or neat PCL in how it interacts with lipase molecules, potentially leading to more efficient catalysis.

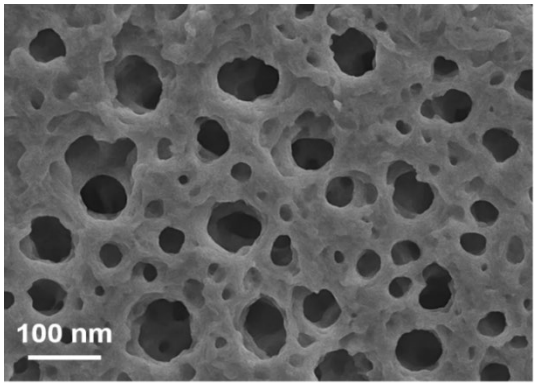

Fig. 7. SEM micrograph of the surface of PCL/3%M-ZnO composite after 14 days of enzymatic degradation with lipase.

Degradation in soil is a complex process involving a consortium of microorganisms, varying moisture levels, and temperature fluctuations, alongside abiotic hydrolysis.30 After 180 days of soil burial, neat PCL showed a weight loss of 40.1%. The PCL/3%U-ZnO composite exhibited a slightly lower weight loss of 38.5%. This might be due to the antimicrobial properties of ZnO 6 [55], where the release of Zn^{2+} ions from the less protected U-ZnO could inhibit the activity of some soil microorganisms responsible for PCL degradation, at least initially. In contrast, the PCL/3%M-ZnO composite showed the highest weight loss of 48.3% after 180 days. This suggests that while M-ZnO also possesses antimicrobial potential, its better dispersion and encapsulation within the PCL matrix due to the APTES coating might lead to a more controlled (possibly lower initial) release of Zn^{2+}. More importantly, the improved interface and potentially altered PCL morphology (e.g., increased surface area due to better filler dispersion, or changes in spherulitic structure) in PCL/M-ZnO might eventually create more sites susceptible to microbial attack or facilitate better moisture penetration, leading to enhanced overall degradation over extended periods [56]. SEM analysis of the PCL/3%M-ZnO surface after 90 days of soil burial (Figure 8) revealed evidence of microbial colonization, surface cracking, and fragmentation of the film.

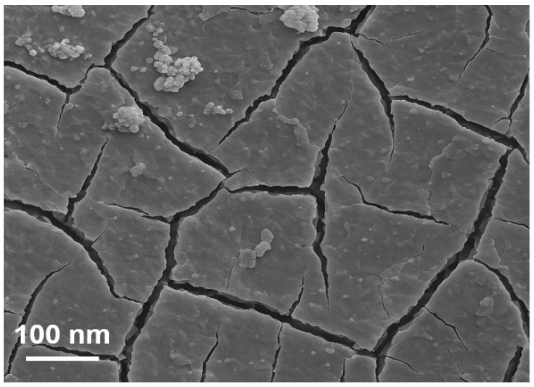

Fig. 8. SEM micrograph of the surface of PCL/3%M-ZnO composite after 90 days of soil burial.

3.3. Overall discussion: structure-property-degradation relationships

The results consistently demonstrate that the APTES surface modification of ZnO nanoparticles plays a crucial role in determining the microstructure, mechanical performance, and degradation behavior of PCL/ZnO nanocomposites. The successful grafting of APTES onto ZnO, confirmed by FTIR, TGA, and TEM of the nanoparticles, translated directly into improved dispersion and significantly enhanced interfacial adhesion within the PCL matrix, as visualized by SEM of the composite fracture surfaces. This improved microstructure is the primary reason for the superior mechanical properties observed in PCL/M-ZnO composites. The well-bonded and well-dispersed M-ZnO nanoparticles act as effective stress transfer agents, efficiently carrying load from the PCL matrix, leading to substantial increases in Young's modulus and tensile strength compared to both neat PCL and PCL/U-ZnO composites. The agglomerated U-ZnO particles, with their weak interfacial bonding, were far less effective as reinforcement and, at higher concentrations, likely acted as defect sites. The increased crystallinity of PCL in the presence of M-ZnO, observed through XRD and DSC, also contributes to the enhanced stiffness and strength. M-ZnO nanoparticles, due to their better dispersion and modified surface chemistry, serve as more effective heterogeneous nucleating agents than U-ZnO. This altered crystalline architecture can also influence degradation, as crystalline domains are generally more resistant to attack than amorphous regions.

The impact on biodegradability is more nuanced. In hydrolytic and enzymatic degradation, PCL/M-ZnO composites generally exhibited faster degradation rates. This could be attributed to the increased interfacial area created by well-dispersed nanoparticles providing more pathways for water ingress or enzyme access to the PCL chains. The modified surface chemistry of M-ZnO might also promote better wetting by aqueous media or more favorable enzyme adsorption. In soil burial, the initial antimicrobial effect of ZnO might play a role, but over longer periods, the enhanced surface area and potentially altered matrix morphology in PCL/M-ZnO composites appeared to facilitate greater overall degradation.

It is important to recognize that the pursuit of optimal ZnO surface modification may involve trade-offs. For instance, an extremely strong interfacial bond that maximizes mechanical strength might, in some circumstances, overly restrict PCL chain mobility or shield PCL segments from enzymatic or hydrolytic attack in the immediate vicinity of the nanoparticles. This could lead to a situation where maximizing one property (e.g., strength) might not concurrently maximize another

(e.g., degradation rate under specific conditions). Thus, the "ideal" composite formulation and modification strategy will ultimately depend on the specific balance of mechanical performance and degradation profile required for a given application. Furthermore, the long-term stability of the APTES coating itself during prolonged degradation, particularly in the complex soil environment, is a factor to consider. Hydrolysis or degradation of the silane layer over extended periods could alter the nature of the PCL-filler interface, potentially changing the degradation mechanism or rate in the later stages of the material's lifecycle. This aspect warrants further investigation for applications requiring very long-term stability or predictable multi-stage degradation. To visually summarize the complex interplay among nanoparticle surface modification, interfacial microstructure, and biodegradation behavior, a schematic representation is provided in Figure 9.

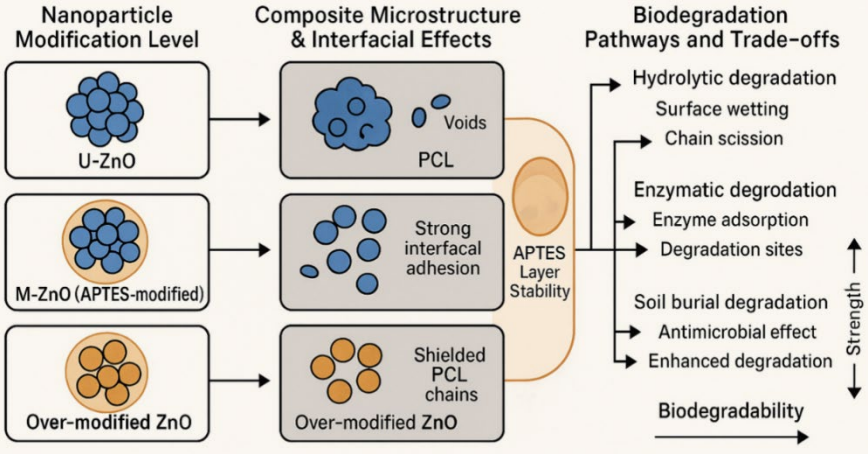

Fig. 9. A mechanistic representation showing how ZnO surface modification alters filler dispersion, interfacial interactions, and thereby influences the degradation behavior of PCL/ZnO nanocomposites through multiple pathways.

4. Conclusion

This research successfully demonstrated the significant impact of APTES surface modification of ZnO nanoparticles on the mechanical strength and biodegradation characteristics of PCL composite materials. FTIR, TGA, and TEM analyses confirmed the effective grafting of APTES onto the ZnO nanoparticle surfaces. This surface modification led to a marked improvement in the dispersion of ZnO nanoparticles and enhanced interfacial adhesion within the PCL matrix, as evidenced by SEM observations, when compared to composites containing unmodified ZnO.

The enhanced microstructure of PCL/M-ZnO composites translated directly into superior mechanical properties. For example, the PCL composite containing 3 wt% M-ZnO exhibited a tensile strength of 35.2 MPa and a Young's modulus of 558 MPa, representing improvements of approximately 73% and 77%, respectively, over neat PCL, and 46% and 39% over PCL with 3 wt% unmodified ZnO (PCL/U-ZnO). These enhancements are attributed to efficient stress transfer from the PCL matrix to the well-dispersed, strongly-bonded M-ZnO nanoparticles and an increase in PCL crystallinity.

The biodegradation studies revealed that ZnO surface modification also influenced the degradation behavior of PCL. PCL/M-ZnO composites generally exhibited accelerated degradation rates under enzymatic conditions (e.g., 36.1% weight loss for PCL/3%M-ZnO vs. 21.3% for neat PCL after 14 days with lipase) and slightly increased hydrolytic degradation. In soil burial tests, PCL/M-ZnO composites showed the highest weight loss after 180 days (48.3% for PCL/3%M-ZnO), suggesting that factors such as improved interfacial water transport and potentially altered microbial interactions due to the modified surface and better dispersion outweigh initial antimicrobial effects over longer durations.

The findings underscore the critical importance of nanoparticle surface modification in optimizing the overall performance of PCL-based nanocomposites. The developed PCL/M-ZnO composites, with their enhanced mechanical strength and tunable biodegradability, show promise for advanced applications such as biomedical scaffolds requiring robust mechanical integrity and controlled resorption rates, or as durable, eco-friendly packaging materials with more predictable end-of-life characteristics.

Future research should focus on exploring the effects of different types of silane coupling agents with varying organic chain lengths or alternative functional groups to further tailor interfacial properties. Investigating the in vivo degradation and comprehensive biocompatibility of these PCL/M-ZnO composites is essential for their translation into biomedical applications. Furthermore, exploring scalable melt processing techniques for composite fabrication and conducting detailed studies on the long-term environmental fate and ecotoxicity of the nanoparticles released after PCL matrix degradation would provide valuable insights for sustainable material design.

Acknowledgements

This work was supported by Key project of science and technology research program of Chongqing Education Commission of China (No. KJZD-K202403601)

References

[1] A. Samir, F. H. Ashour, A. A. A. Hakim, M. Bassyouni, npj Materials Degradation 6, 68 (2022); https://doi.org/10.1038/s41529-022-00277-7

[2] M. Labet, W. Thielemans, Chemical Society Reviews 38, 3484 (2009); https://doi.org/10.1039/b820162p

[3] S. Homaeigohar, A. R. Boccaccini, Frontiers in Chemistry 9, 809676 (2022); https://doi.org/10.3389/fchem.2021.809676

[4] D. Mondal, M. Griffith, S. S. Venkatraman, International Journal of Polymeric Materials and Polymeric Biomaterials 65, 255 (2016); https://doi.org/10.1080/00914037.2015.1103241

[5] J. Hu, Y. Song, C. Zhang, W. Huang, A. Chen, H. He, S. Zhang, Y. Chen, C. Tu, J. Liu, X. Xuan, Y. Chang, J. Zheng, J. Wu, ACS Applied Bio Materials 3, 965 (2020); https://doi.org/10.1021/acsabm.9b01000

[6] Q. Wang, W. Chen, W. Zhu, D. J. McClements, X. Liu, F. Liu, npj Science of Food 6, 18 (2022); https://doi.org/10.1038/s41538-022-00132-8

[7] N. Yang, L. Ying, K. Li, F. Chen, F. Zhao, Z. Sun, L. Feng, J. Liu, Polymers 14, 5340 (2022); https://doi.org/10.3390/polym14245340

[8] E. Malikmammadov, T. E. Tanir, A. Kiziltay, V. Hasirci, N. Hasirci, Journal of Biomaterials

Science, Polymer Edition 29, 863 (2018); https://doi.org/10.1080/09205063.2017.1394711
[9] N. Alharbi, M. Guthold, Journal of the Mechanical Behavior of Biomedical Materials 155, 106564 (2024); https://doi.org/10.1016/j.jmbbm.2024.106564
[10] H. Sun, L. Mei, C. Song, X. Cui, P. Wang, Biomaterials 27, 1735 (2006); https://doi.org/10.1016/j.biomaterials.2005.09.019
[11] J. R. Dias, A. Sousa, A. Augusto, P. J. Bártolo, P. L. Granja, Polymers 14, 3397 (2022); https://doi.org/10.3390/polym14163397
[12] S. Cheng, S.-J. Xie, J.-M. Y. Carrillo, B. Carroll, H. Martin, P.-F. Cao, M. D. Dadmun, B. G. Sumpter, V. N. Novikov, K. S. Schweizer, A. P. Sokolov, ACS Nano 11, 752 (2017); https://doi.org/10.1021/acsnano.6b07172
[13] S. Z. Al Sheheri, Z. M. Al-Amshany, Q. A. Al Sulami, N. Y. Tashkandi, M. A. Hussein, R. M. El-Shishtawy, Designed Monomers and Polymers 22, 8 (2019); https://doi.org/10.1080/15685551.2019.1565664
[14] I. Keun Kwon, S. Kidoaki, T. Matsuda, Biomaterials 26, 3929 (2005); https://doi.org/10.1016/j.biomaterials.2004.10.007
[15] B. Zhang, X. Chen, W. Lu, Q. M. Zhang, J. Bernholc, Nanoscale 13, 10933 (2021); https://doi.org/10.1039/D1NR00165E
[16] P. H. C. Camargo, K. G. Satyanarayana, F. Wypych, Materials Research 12, 1 (2009); https://doi.org/10.1590/S1516-14392009000100002
[17] N. P. Shetti, S. D. Bukkitgar, K. R. Reddy, Ch. V. Reddy, T. M. Aminabhavi, Biosensors & Bioelectronics 141, 111417 (2019); https://doi.org/10.1016/j.bios.2019.111417
[18] D. K. Sharma, S. Shukla, K. K. Sharma, V. Kumar, Materials Today Proceedings 49, 3028 (2022); https://doi.org/10.1016/j.matpr.2020.10.238
[19] T. Smijs, Pavel, Nanotechnology, Science and Applications 95 (2011); https://doi.org/10.2147/NSA.S19419
[20] C. Contado, Frontiers in Chemistry 3, (2015); https://doi.org/10.3389/fchem.2015.00048
[21] Y. Ahmadzadeh, A. Babaei, A. Goudarzi, Polymer Degradation and Stability 158, 136 (2018); https://doi.org/10.1016/j.polymdegradstab.2018.10.007
[22] N. Johari, F. Rafati, F. Zohari, P. G. Tabari, A. Samadikuchaksaraei, Materials Chemistry and Physics 280, 125786 (2022); https://doi.org/10.1016/j.matchemphys.2022.125786
[23] J. I. Castro, D. G. Araujo-Rodríguez, C. H. Valencia-Llano, D. López Tenorio, M. Saavedra, P. A. Zapata, C. D. Grande-Tovar, Pharmaceutics 15, 2196 (2023); https://doi.org/10.3390/pharmaceutics15092196
[24] L. Vannozzi, P. Gouveia, P. Pingue, C. Canale, L. Ricotti, ACS Applied Materials & Interfaces 12, 21398 (2020); https://doi.org/10.1021/acsami.0c00154
[25] Y. Zare, Computational Materials Science 111, 334 (2016); https://doi.org/10.1016/j.commatsci.2015.09.053
[26] H. Ennaceri, L. Wang, D. Erfurt, W. Riedel, G. Mangalgiri, A. Khaldoun, A. El Kenz, A. Benyoussef, A. Ennaoui, Surface and Coatings Technology 299, 169 (2016); https://doi.org/10.1016/j.surfcoat.2016.04.056
[27] R. Hong, T. Pan, J. Qian, H. Li, Chemical Engineering Journal 119, 71 (2006); https://doi.org/10.1016/j.cej.2006.03.003
[28] K. Roy, Md. N. Alam, S. K. Mandal, S. C. Debnath, Journal of Nanostructure in Chemistry 4, 133 (2014); https://doi.org/10.1007/s40097-014-0127-9
[29] T. Aziz, A. Ullah, H. Fan, M. I. Jamil, F. U. Khan, R. Ullah, M. Iqbal, A. Ali, B. Ullah, Journal of Polymers and the Environment 29, 3427 (2021); https://doi.org/10.1007/s10924-021-02142-1
[30] Y. Zhang, C. Wang, F. Liu, X. Sun, X. Guo, L. Zhao, G. Lu, Sensors and Actuators, B: Chemical 363, 131845 (2022); https://doi.org/10.1016/j.snb.2022.131845
[31] R. G. Acres, A. V. Ellis, J. Alvino, C. E. Lenahan, D. A. Khodakov, G. F. Metha, G. G. Andersson, Journal of Physical Chemistry C 116, 6289 (2012); https://doi.org/10.1021/jp212056s
[32] A. F. Jaramillo, R. Baez-Cruz, L. F. Montoya, C. Medinam, E. Pérez-Tijerina, F. Salazar, D.

Rojas, M. F. Melendrez, Ceramics International 43, 11838 (2017); https://doi.org/10.1016/j.ceramint.2017.06.027

[33] Department of Materials Science, Institute of Graduate Studies and Research, Alexandria University, 163 Horrya Avenue, El-Shatby, P.O. Box 832, Alexandria, Egypt, Z. Mohamed, M. Soliman, Department of Materials Science, Institute of Graduate Studies and Research, Alexandria University, 163 Horrya Avenue, El-Shatby, P.O. Box 832, Alexandria, Egypt, A. Gad, Department of Materials Science, Institute of Graduate Studies and Research, Alexandria University, 163 Horrya Avenue, El-Shatby, P.O. Box 832, Alexandria, Egypt, S. M. Ebrahim, Department of Materials Science, Institute of Graduate Studies and Research, Alexandria University, 163 Horrya Avenue, El-Shatby, P.O. Box 832, Alexandria, Egypt, Y. Elkony, and Heavy Metal lab, Central labs of Ministry of Health, Alexandria, Egypt, Integrated Nano 1, 10 (2024); https://doi.org/10.62184/in.jin010420244

[34] N. Majoul, S. Aouida, B. Bessaïs, Applied Surface Science 331, 388 (2015); https://doi.org/10.1016/j.apsusc.2015.01.107

[35] N. N. Rabin, J. Morshed, H. Akhter, Md. S. Islam, Md. A. Hossain, M. Elias, Md. M. Alam, M. R. Karim, M. A. Hasnat, Md. N. Uddin, I. A. Siddiquey, International Journal of Chemical Reactor Engineering 14, 785 (2016); https://doi.org/10.1515/ijcre-2015-0141

[36] S. Raha, Md. Ahmaruzzaman, Nanoscale Advances 4, 1868 (2022); https://doi.org/10.1039/D1NA00880C

[37] W. Zhang, E. P. C. Lai, Silicon 14, 6535 (2022); https://doi.org/10.1007/s12633-021-01477-7

[38] G. Saber, A. El-Dissouky, G. Badie, S. Ebrahim, A. Shokry, RSC Advances 13, 16453 (2023); https://doi.org/10.1039/D3RA00491K

[39] Y. Chen, Q. Duan, J. Zhu, H. Liu, L. Chen, L. Yu, Carbohydrate Polymers 272, 118450 (2021); https://doi.org/10.1016/j.carbpol.2021.118450

[40] D. S. Nakonieczny, F. Kern, L. Dufner, A. Dubiel, M. Antonowicz, K. Matus, Materials 14, 6651 (2021); https://doi.org/10.3390/ma14216651

[41] R. S. Alruwais, W. A. Adeosun, H. M. Marwani, M. Jawaid, A. M. Asiri, A. Khan, Polymers 13, 2562 (2021); https://doi.org/10.3390/polym13152562

[42] R. Mahdavi, S. S. A. Talesh, Journal of Alloys and Compounds 896, 163121 (2022); https://doi.org/10.1016/j.jallcom.2021.163121

[43] L. A. Montejo-Mesa, A. M. Díaz-García, C. L. Cavalcante, E. Vilarrasa-García, E. Rodríguez-Castellón, D. Ballesteros-Plata, G. I. Autié-Castro, Molecules 29, 5219 (2024); https://doi.org/10.3390/molecules29215219

[44] Z. Gončuková, M. Řezanka, J. Dolina, L. Dvořák, Reactive and Functional Polymers 162, 104872 (2021); https://doi.org/10.1016/j.reactfunctpolym.2021.104872

[45] A. Mukherjee, B. Dasgupta Ghosh, Polymer Composites 44, 2488 (2023); https://doi.org/10.1002/pc.27258

[46] N. Khurana, P. Arora, A. S. Pente, K. C. Pancholi, V. Kumar, C. P. Kaushik, S. Rattan, Inorganic Chemistry Communications 124, 108347 (2021); https://doi.org/10.1016/j.inoche.2020.108347

[47] D. Prodan, M. Moldovan, G. Furtos, C. Saroși, M. Filip, I. Perhaița, R. Carpa, M. Popa, S. Cuc, S. Varvara, D. Popa, Applied Sciences 11, 11330 (2021); https://doi.org/10.3390/app112311330

[48] M. Sypabekova, A. Hagemann, D. Rho, S. Kim, Biosensors 13, 36 (2023); https://doi.org/10.3390/bios13010036

[49] S. Aliakbarshirazi, R. Ghobeira, T. Egghe, N. De Geyter, H. Declercq, R. Morent, Applied Surface Science 640, 158380 (2023); https://doi.org/10.1016/j.apsusc.2023.158380

[50] M. Sohrabian, S. Ranjbareslamloo, B. Arab, M. Vaseghi, Computational Materials Science 255, 113930 (2025); https://doi.org/10.1016/j.commatsci.2025.113930

[51] Z. Hussain, S. Ullah, J. Yan, Z. Wang, I. Ullah, Z. Ahmad, Y. Zhang, Y. Cao, L. Wang, M. Mansoorianfar, R. Pei, Chemosphere 307, 135810 (2022); https://doi.org/10.1016/j.chemosphere.2022.135810

[52] M. Tavira, M. Mousavi-Khattat, Z. Shakeran, A. Zarrabi, International Journal of

Pharmaceutics 642, 123162 (2023); https://doi.org/10.1016/j.ijpharm.2023.123162
[53] A. Ressler, L. Bauer, T. Prebeg, M. Ledinski, I. Hussainova, I. Urlić, M. Ivanković, H. Ivanković, Materials 15, 3348 (2022); https://doi.org/10.3390/ma15093348
[54] J. Lai, H. Huang, M. Lin, Y. Xu, X. Li, B. Sun, Frontiers in Microbiology 13, 1113705 (2023); https://doi.org/10.3389/fmicb.2022.1113705
[55] R. Kumar, A. Umar, G. Kumar, H. S. Nalwa, Ceramics International 43, 3940 (2017); https://doi.org/10.1016/j.ceramint.2016.12.062
[56] Y. Kaptan, Y. Güvenilir, European Journal of Pharmaceutics and Biopharmaceutics 181, 60 (2022); https://doi.org/10.1016/j.ejpb.2022.11.001